Ryu *et al. Molecular Cancer* (2024) 23:227
https://doi.org/10.1186/s12943-024-02138-0

Molecular Cancer

RESEARCH Open Access

Chaperone-mediated autophagy modulates Snail protein stability: implications for breast cancer metastasis

Ki-Jun Ryu[1†], Ki Won Lee[1†], Seung-Ho Park[2], Taeyoung Kim[1], Keun-Seok Hong[1], Hyemin Kim[1], Minju Kim[1], Dong Woo Ok[1], Gu Neut Bom Kwon[1], Young-Jun Park[2], Hyuk-Kwon Kwon[1,3], Cheol Hwangbo[1,3], Kwang Dong Kim[1,3], J. Eugene Lee[4] and Jiyun Yoo[1,3*]

Abstract

Breast cancer remains a significant health concern, with triple-negative breast cancer (TNBC) being an aggressive subtype with poor prognosis. Epithelial-mesenchymal transition (EMT) is important in early-stage tumor to invasive malignancy progression. Snail, a central EMT component, is tightly regulated and may be subjected to proteasomal degradation. We report a novel proteasomal independent pathway involving chaperone-mediated autophagy (CMA) in Snail degradation, mediated via its cytosolic interaction with HSC70 and lysosomal targeting, which prevented its accumulation in luminal-type breast cancer cells. Conversely, Snail predominantly localized to the nucleus, thus evading CMA-mediated degradation in TNBC cells. Starvation-induced CMA activation downregulated Snail in TNBC cells by promoting cytoplasmic translocation. Evasion of CMA-mediated Snail degradation induced EMT, and enhanced metastatic potential of luminal-type breast cancer cells. Our findings elucidate a previously unrecognized role of CMA in Snail regulation, highlight its significance in breast cancer, and provide a potential therapeutic target for clinical interventions.

Keywords Chaperone-mediated autophagy, Snail, EMT, Metastasis, Breast cancer

Background

Breast cancer, the most frequent malignancy among women accounts for about 30% of all cancer cases and 15% of all cancer deaths in women [1, 2]. Triple-negative breast cancers (TNBC) manifest heightened aggressiveness and dismal prognoses among the diverse subtypes of breast carcinoma [3]. These aggressive tumors relapse frequently, are more prone to metastasize, and have worse outcomes than those observed in other breast cancer types [4, 5].

Most cancer-related deaths result from local invasion and distant metastasis [6], which involves loss of apical-basal polarity and intercellular contact in epithelial cells causing a shift to a mesenchymal phenotype [7]. This is

†Ki-Jun Ryu and Ki Won Lee contributed equally to this work.

*Correspondence:
Jiyun Yoo
yooj@gsnu.ac.kr
[1]Division of Applied Life Science (Brain Korea 21 Four), Research Institute of Life Sciences, Gyeongsang National University, Jinju 52828, Korea
[2]Environmental Disease Research Center, Korea Research Institute of Bioscience and Biotechnology, Daejeon 34141, Korea
[3]Division of Life Science, College of Natural Sciences, Gyeongsang National University, Jinju 52828, Korea
[4]Division of Biometrology, Korea Research Institute of Standards and Science, Daejeon 34113, Korea

accompanied by increased cell motility and expression of mesenchymal genes, a process known as epithelial-mesenchymal transition (EMT), a key step in tumor progression towards metastasis [8, 9]. EMT regulators play important roles in cancer progression, including the zinc finger protein Snail, which induces EMT by directly downregulating E-cadherin transcription during tumor development and progression [10, 11]. Elevated expression of Snail correlates with advanced tumor grade, metastasis, recurrence, and dismal prognosis in breast cancer patients [12–14].

Snail is a labile protein that rapidly undergoes proteasomal degradation post glycogen synthase kinase-3β (GSK-3β)-dependent phosphorylation and β-TrCP1-mediated ubiquitination [15]. Snail protein contains two GSK-3β consensus sites, of which one is phosphorylated at four serine residues adjacent to a nuclear export sequence (NES) by GSK-3β, leading to the subsequent unmasking of protein and export from the nucleus [16]. The second site is phosphorylated by GSK-3β in the cytosol at two serine residues that overlap with a destruction motif recognized by the E3 ubiquitin ligase β-TrCP1. Phosphorylated Snail binds to β-TrCP1, and undergoes ubiquitination and degradation [15]. Recent studies have reported the role of GSK-3β-dependent Snail phosphorylation in SPSB3-, FBW7-, FBXO22-, and FBXO31-mediated Snail ubiquitination and degradation [17–20]. Several E3 ubiquitin ligases ubiquitinate Snail in the cytosol, leading to proteasomal degradation, which suggests Snail protein has greater stability in the nucleus than that in the cytosol [21–25]. Notably, kinases, including ERK2, PAK1, Lats2, and p38 either translocate cytosolic Snail to the nucleus or retain it within the nucleus, thereby avoiding ubiquitination and degradation [26–29]. However, the recent discovery of FBXL5, an E3 ubiquitin ligase that target nuclear Snail [30], has rendered the hypothesis of the high stability of nuclear Snail less compelling.

Chaperone-mediated autophagy (CMA) is a selective autophagy mechanism that relies on lysosomal degradation of cytosolic proteins [31]. Cellular proteins that contain a recognition motif chemically related to the pentapeptide Lys-Phe-Glu-Arg-Gln (KFERQ) are recognized by cytoplasmic heat-shock chaperone HSC70 and its associated co-chaperones, before being targeted to the lysosome membrane. The substrate is translocated via the membrane into the lysosomal lumen post interaction with the lysosome-associated membrane protein type 2 A (LAMP2A), and degraded by intraluminal proteases [32, 33]. We demonstrate that Snail degradation by cytosolic CMA is independent of proteasomal degradation in luminal-type breast cancer cells with low Snail expression. We further show the nuclear retention of Snail in TNBC cells, unlike that in luminal-type breast cancer cells, aids evasion of CMA-mediated degradation. Our findings highlight chaperone-mediated autophagy (CMA) as an unrecognized mechanism that governs Snail protein turnover, and sheds light on the complex regulation of Snail stability and its implications in breast cancer progression.

Materials and methods

Cell culture

All cell lines used in this study were obtained from the Korean Cell Line Bank (KCLB, Seoul, Korea), where they were characterized by DNA-fingerprinting and isozyme detection, and cultured according to American Type Culture Collection instructions. All cell lines were used within 3 to 20 passages of thawing the original stocks and were tested every 3 months for mycoplasma contamination. The cell lines were maintained for no more than 3 passages between experiments. Human HEK293T and human breast cancer cell lines (MCF-7, MDA-MB 231) were cultured in DMEM (Invitrogen, Carlsbad, CA, USA) supplemented with 10% FBS and 1% penicillin and streptomycin. Human breast cancer cell lines (T47D, BT549) were cultured in RPMI (Invitrogen, Carlsbad, CA, USA) supplemented with 10% FBS and 1% penicillin and streptomycin. Serum starvation experiments were performed by switching from normal medium to medium containing 0.2% FBS after 24 h of incubation and maintaining the culture for an additional 48 h.

Plasmid construction and transfection

The wild type Snail, HSC70, and LAMP2A plasmids were purchased from Sino Biological (Beijing, China). Site-directed mutagenesis was performed with a QuikChange mutagenesis kit (Stratagene, San Diego, CA, USA), according to the manufacturer's instructions. For transient transfection, HEK293T cells were seeded in 6-well or 100-mm-diameter dish for 24 h and transfected with the indicated plasmid by using X-tremeGENE™ HP DNA transfection reagent (Roche, Basel, Switzerland) following manufacturer's instruction. After 48 h, the cells were harvested and used for western blot analysis. Two different siRNA oligo duplexes for targeting human HSC70 (siHSC70-1; 5'-GCUGGUCUCAAUGUACUUATT-3' and siHSC70-2; 5'-GUGCCAUGACAAAGGAUAATT-3'), LAMP2A (siLAMP2A-1; 5'-GCAGUGCAGAUGACGACAATT-3' and siLAMP2A-2; 5'-GCCUUGGCAGGAGUACUUATT-3'), LAMP2B (siLAMP2B; 5'-GUGUUCGCUGGAUGAUGACACCATT-3') or ATG7 (siATG7-1; 5'-CAGCUAUUGGAACACUGUATT-3' and siATG7-2; 5'-CUCUUGAAAACCCUGUACUTT-3'), respectively, were purchased from Bioneer (Daejeon, Korea). Transient transfection of siRNA oligo duplex was accomplished using Lipofectamine™ RNAiMAX Transfection Reagent (Invitrogen, Carlsbad, CA, USA) following manufacturer's instruction. For stable transfection,

MCF-7 cells were transfected with Flag-tag (Control), Flag-WT-Snail, or Flag-58AAAA-Snail expressing plasmid by using the X-tremeGENE™ HP DNA transfection reagent (Roche, Basel, Switzerland). After 48 h incubation, 500 μg/ml of G418 (Sigma, St. Louis, MO, USA) was added to the cultures to select for G418-resistant clones. Three to four weeks later, independent colonies were picked using cloning cylinder (Sigma, St. Louis, MO, USA), sub-cultured, and tested for Snail expression by western blot analysis.

Immunoprecipitation

Cells were lysed in lysis buffer: 20 mM Tris pH 7.4, 2 mM EDTA, 150 mM sodium chloride, 1 mM sodium deoxycholate, 1% Triton X-100, 10% glycerol, 2 pills protease inhibitor cocktail (Roche, Basel, Switzerland), mixed by vortexing and incubated 30 min on ice. Lysates were precleared using protein A/G beads (Santa Cruz Biotechnology, Dallas, Texas, USA), incubated with the specific antibodies for overnight at 4 °C with gentle mixing and then incubated with beads for 2 h at 4 °C with gentle mixing. Beads were then washed 5 times with lysis buffer and eluted with 40 μl of 2 × SDS sample buffer. Western blot analysis was then performed. Primary antibodies used for IP were as follows: anti-Flag (Abm #G191; 2 μg/ml), anti-HA (Abm #G036; 2 μg/ml), mouse mAb IgG1 isotype control (Cell Signaling #5415; 2 μg/ml), anti-HSC70 (Santa Cruz Biotechnology, #sc-7298; 2 μg/ml) and anti-Snail (Cell Signaling #3895; 2 μg/ml).

Western blot analysis

Protein samples were subjected to SDS-PAGE and transferred to polyvinylidene fluoride (PVDF) membranes. Membranes were incubated with indicated primary antibodies for overnight at 4 °C. After washing with TBS-T (TBS containing 0.1% Tween-20), membranes were incubated with corresponding horseradish peroxidase (HRP)-conjugated secondary antibodies (1:5,000) for 1 h at room temperature. Blots were developed with enhanced chemiluminescence (ECL, Bio-Rad, Hercules, CA, USA) reaction according to manufacturer's instructions. Primary antibodies used were: anti-Snail (Cell Signaling, #3879; 1:1,000), anti-HSC70 (Santa Cruz Biotechnology, #sc-7298; 1:500), anti-LAMP2A (Abcam. #ab125068; 1:1000), anti-LAMP2B (Abcam. #ab18529; 1:1000), anti-LAMP1 (Cell Signaling, #9091; 1:1,000), anti-Flag (Abm, #G191; 1:2,000), Monoclonal ANTI-FLAG® M2-Peroxidase (HRP) (Sigma-Aldrich, #A8592; 1:2,000), anti-HA (Abm, #G036; 1:2,000), anti-HA High Affinity (Roche, #11867423001; 1:1,000), anti-Histone H3 (Cell Signaling, #4499; 1:1,000), anti-α-tubulin (Sigma-Aldrich, #T6199; 1:10,000), anti-β-actin (Cell Signaling, #4967; 1:1,000), anti-LC3B (Cell Signaling, #3868; 1:1,000), anti-Ubiquitin (linkage-specific K48) (Abcam. #ab18529; 1:1,000), anti-ATG7 (Cell Signaling, #8558; 1:1,000), anti-p62/SQSTM1 (Sigma-Aldrich, #P0067; 1:1,000), anti-MEK1/2 (Cell Signaling, #8727; 1:1,000), anti-Lamin A/C (Santa Cruz Biotechnology, #sc-376248; 1:500), anti-E-cadherin (BD Biosciences, #610181; 1:10,000), anti-Occludin (Invitrogen, #71-1500; 1:1,000), anti-ZO-1 (Invitrogen, #40-2200; 1:1,000), anti-Fibronectin (BD Biosciences, #610078; 1:5,000), anti-N-cadherin (BD Biosciences, #610921; 1:5,000), anti-Vimentin (Santa Cruz Biotechnology, #sc-6260; 1:500), anti-Claudin-1 (Cell Signaling, #13995; 1:1,000), anti-p-PKD1 (Ser744/748) (Cell Signaling, #2054; 1:1,000), anti-PKD1 (Cell Signaling, #90039; 1:1,000), anti-p-PAK1 (Thr423)/PAK2 (Thr402) (Cell Signaling, #2601; 1:1,000), anti-PAK1 (Cell Signaling, #2602; 1:1,000), anti-GSK3β (Ser9) (Cell Signaling, #5558; 1:1,000), anti- GSK3β (Cell Signaling, #9315; 1:1,000), anti-p-Akt (Ser473) (Cell Signaling, #9271; 1:1,000), anti-Akt (Cell Signaling, #9272; 1:1,000).

Total RNA extraction and qRT-PCR

Total RNA was extracted from the cultured cells using RNeasy Mini Kit (GeneAll, Seoul, Korea) following the manufacturer's instructions. Reverse transcription was performed using iScript™ cDNA synthesis kit (Bio-Rad, Hercules, CA, USA) following the manufacturer's instructions. qRT-PCR was performed using iQ™ SYBR®q RT/PCR PreMix (Bio-Rad, Hercules, CA, USA) following the manufacturer's instructions. Amplification was performed using CFX96 Touch Real-Time Detection System. Primers used were: Snail (F: 5'-ATCGGAAGCCTAACT ACAGC-3'; R: 5'-CAGAGTCCCAGATGAGCATT-3'), GAPDH (F: 5'-GTGGTCTCCTCTGACTTCAAC-3'; R: 5'-TCTCTTCCTCTTGTGCTCTTG-3').

Immunofluorescence and confocal microscopy

The cells were washed once in PBS and then fixed in fresh 4% paraformaldehyde at room temperature for 15 min. To ensure permeability and prevent non-specific antibody binding, the cells were treated with PBS containing 0.1% Triton X-100 and 5% bovine serum albumin (BSA) for 1 h. Following that, the cells were incubated overnight at 4 °C with the appropriate antibody. The cells were washed four times with PBS and then incubated for 1 h with Alexa Fluor-conjugated secondary antibodies (Invitrogen, Carlsbad, CA, USA). Samples were washed and mounted on microscope slides with a drop of VECTASHIELD (Vector Labs, Newark, CA, USA) and sealed with medical adhesive. Samples were examined with laser-scanning confocal microscope (Olympus, Japan).

Cycloheximide (CHX) pulse-chase assay

HEK293T and MCF-7 stable cells were seeded on 12-well plate at a density of 2.5×10^5 cells per well. After culturing overnight, the cells were transfected with plasmids or

siRNAs or treated with inhibitors as desired. Two days after transfection, the cells were treated with 100 μg/ml of cycloheximide before harvest. Total protein lysates were collected at different time points and subjected to immunoblotting for Snail.

Ubiquitination assay

Ubiquitination assay was done following an immunoprecipitation protocol. After culturing overnight, HEK293T cells were transfected with plasmids or siRNAs as desired. Two days after transfection, cells were treated with 10 μM MG132 (Sigma-Aldrich, #C2211) for 8 h to block proteasomal degradation of the Snail protein before lysed with Triton X-100 lysis buffer. Cell lysates were then collected and immunoprecipitated with anti-Flag antibody (Abm, #G191; 2 μg/ml) to specifically pull-down Flag-Snail protein. Pulled down samples were subject to immunoblotting with anti-HA (Ubiquitin) to visualize polyubiquitinated Snail protein bands.

Cellular fractionation and lysosome isolation

HEK293T cells were cultured at a density of 1×10^6cells per dish in 100 mm diameter dishes and transfected with plasmids 24 h later. After 48 h of cultivation, cells were harvested. 12 h before cell harvest, the cells were treated with NH_4Cl (Sigma-Aldrich, #A9434; 20 mM) and leupeptin (Santa Cruz Biotechnology, #sc-295358; 100 μM). Cellular fractionation was carried out using the NE-PER™ Nuclear and Cytoplasmic Extraction Reagents (Thermo Fisher Scientific, #78835) following the manufacturer's instructions. Lysosome isolation was performed using the Minute™ Lysosome Isolation Kit for Mammalian Cells/Tissues (Invent, #LY-034) following the manufacturer's instructions.

Proliferation assay

Cells were seeded in 6-well plates at 1×10^5 cells/well. After incubation for 1 to 4 days, cells were trypsinized and resuspended in 1 ml of appropriate medium. The viable cells were stained with trypan blue and counted with a hemocytometer.

Migration assay

Cells were seeded into Culture-Insert (Ibidi, Fitchburg, WI, USA) at 5×10^5 cells/insert. After the cells were confluent, the Culture-Insert was removed and washed with PBS for three times to rinse off the detached cells. Cells were then cultured with appropriate fresh media for further 24 h. The wound closure was observed and photographed at indicated times, using a phase-contrast microscope with digital camera.

Invasion assay

Invasion assays were assessed using QCM™ 24-Well Cell Invasion Assay (Fluorometric) kit (Millipore, Bedford, MA, USA) following the manufacturer's instruction. Cells were serum-starved for 24 h and 2.5×10^5 cells in 250 μl of serum-free medium were seeded into upper chambers. The lower chambers were filled with 500 μl of appropriate media containing 20% fetal bovine serum. 30 h after incubation, non-invaded cells/medium remaining on the upper chambers were removed by pipetting. The upper chambers were transferred into a clean well containing 225 μl of prewarmed Cell Detachment Solution, and incubated for 30 min at 37 °C. The upper chambers were removed from the well. 75 μl of Lysis Buffer/Dye solution (CyQuant GR Dye 1:75 with 4X Lysis Buffer) was added into each well and incubated for 15 min at room temperature. Two hundred microliters of the mixture were transferred into a 96-well plate and assessed with a fluorescence plate reader using a 480/520 nm filter set.

Mice and animal housing

Female BALB/c nude mice at 6 weeks of age were purchased from DooYeol Biotech and housed in a pathogen-free barrier room in Animal Care Facility at Korea Research Institute of Bioscience and Biotechnology (KRIBB). All experiments using animals were conducted under the Institutional Animal Care and Use Committee (IACUC)-approved protocols at KRIBB in accordance with institutional guidelines.

Xenografts studies

For metastasis analysis of MCF-7 human breast cancer models, 2×10^6 of MCF-7 (Control), wild-type Snail or mutant Snail-expressing MCF-7 (Snail-WT) and MCF-7 (Snail-58AAAA) cells were injected into the lateral tail-vein of BALB/c female nude mice ($n=7$ for each group). Six weeks after the injection, the mice were euthanized, and stained H&E at lung.

Statistical analysis

Quantitative data in this study are presented as means ± S.D. and were analyzed by Student's t-test, one-way ANOVA or two-way ANOVA. $P<0.05$ was considered statistically significant. For quantification of protein stability following treatment of cycloheximide, Snail and α-tubulin proteins detected by immunoblotting were quantified using ImageJ software. For normalization, α-tubulin expression was used as a control. GraphPad Prism version 7 and SPSS version 26 software were used in this study. All experiments were repeated at least three independent times. Animal studies were performed with adequate n numbers to ensure statistical evaluation. No statistical method was used to predetermine sample size.

Sample size was chosen on the basis of literature in the field.

Results

HSC70 interacts with Snail in the cytosol and decreases its protein stability

Snail is highly expressed in TNBC cell lines, but not in normal or luminal-type breast cancer cell lines (Fig. S1A). Snail was barely detectable in stable Flag-tagged Snail transfectants in MCF-7 cells, a non-invasive luminal-type breast cancer cell line (MCF-7/F-Snail, Fig. S1B). However, its expression increased dramatically on pre-treatment with the proteasome inhibitor MG132 (Fig. S1B), indicating rapid degradation of Flag-tagged Snail via a proteasome-dependent pathway in MCF-7 cells. LC-MS/MS analysis performed to identify Snail-interacting proteins detected 59 proteins that co-immunoprecipitation with Snail (Fig. S1C). Zhu et al. identified 389 proteins that interact with Snail in HEK293T cells [34], of which 7 proteins are same as those identified in this study (Fig. S1D), including EEF1A1 that directly influences Snail function [35]. We focused on HSC70, which influences levels of many proteins in several cancer types [36, 37].

The interaction between HSC70 and Snail was confirmed by reciprocal immunoprecipitation in HEK293T cells co-transfected with vectors encoding HA-HSC70 and/or Flag-Snail (Fig. 1A). Additionally, the interaction between endogenous HSC70 and Snail in MCF-7 and T47D breast cancer cells was confirmed (Fig. 1B). Five truncated-forms of Snail (Fig. S2A), along with full-length HSC70 were co-expressed, followed by IP using an anti-Flag antibody to determine the Snail domain required for HSC70 interaction. All the constructs, excluding the 40–78 amino acids-deleted construct (Snail-Δ40–78), associated with HSC70 (Fig. S2B). Confocal microscopy revealed that exogenously expressed (Fig. 1C) and endogenous (Fig. 1D) HSC70 primarily colocalized with Snail in HEK293T and MCF-7 cell cytoplasm, respectively. Further, immunoprecipitation results post nuclear and cytoplasmic fractionation indicated the predominantly cytoplasmic interaction of these proteins (Fig. 1E).

We further determined the effect of HSC70 on Snail expression. RNAi-mediated HSC70 depletion resulted in elevated endogenous Snail levels in HEK293T, MCF-7, and T47D cells, without influencing its mRNA levels (Fig. 1F). A cycloheximide (CHX) pulse-chase analysis demonstrated that HSC70 depletion markedly extended endogenous Snail half-life (from 15 min to 60 min, Fig. 1G). Database analysis revealed that HSC70 mRNA levels in breast cancer patients were positively correlated with the levels of negatively regulated Snail target genes (E-cadherin, ZO-1, and Occludin), but not with Snail mRNA levels (Fig. 1H). These results suggest that HSC70 may negatively regulate Snail by reducing protein stability.

HSC70 induces Snail protein degradation through lysosome

HSC70 regulates protein stability through the carboxyl terminus of HSC70-interacting protein (CHIP)-mediated ubiquitination, which enables proteasomal degradation of target proteins [38–40]. We recently reported CHIP mediated Snail ubiquitination, and regulation of Snail stability in a chaperone-independent manner [24]. Consistent with our previous results, CHIP interacted with Snail on suppression of HSC70 expression (Fig. S3A). Additionally, the Snail-Δ40–78 mutant that does not interact with HSC70, interacted with CHIP (Fig. S3B), and underwent ubiquitination (Fig. S3C). These results indicate that HSC70-mediated decrease in Snail stability is unrelated to CHIP. Additionally, treatment with MG132 post HSC70 inhibition caused a further increase in Snail expression as compared to that observed post treatment with MG132 alone (Fig. S3D). Further, poly-ubiquitination levels of Snail were not decreased on HSC70 depletion (Fig. S3E). These results suggest that HSC70 may regulate Snail stability in a proteasome-independent manner.

HSC70 regulates protein stability via CMA that causes lysosomal degradation of target proteins [32, 33]. Treatment with ammonium chloride and leupeptin (NL) that blocks lysosomal hydrolysis, or chloroquine (CQ), which inhibits autophagy associated lysosomal degradation, resulted in elevated endogenous Snail protein levels in HEK293T, MCF-7, and T47D cells, without affecting its mRNA levels (Fig. 2A and B). Additionally, immunofluorescent co-staining of Snail and LAMP1, a known lysosomal marker, revealed the lysosomal localization of Snail, which was enhanced post inhibition of lysosomal degradation by NL (Fig. 2C). Further, lysosomal accumulation of Snail was evident post NL treatment (Fig. 2D). Exogenously expressed Snail levels and stability were also enhanced post NL treatment (Fig. 2E and F). These results suggest that Snail may undergo lysosomal degradation. Any additional increase in Snail expression was not evident post NL treatment after HSC70 inhibition as compared to that observed post treatment with NL alone (Fig. 2G). Further, unlike WT-Snail, the expression of the Snail-Δ40–78 mutant was not elevated by NL (Fig. 2H), which indicates that HSC70 may induce lysosomal Snail degradation. MG132 treatment with NL or CQ cumulatively influenced Snail levels in HEK293T (Fig. 2I) and Snail expressing MCF-7 (Fig. 2J) cells, which suggests that lysosomal Snail degradation may be independent of the proteasome.

The treatment of HEK293T cells with 3-methyladenine (3-MA), a well-characterized selective inhibitor

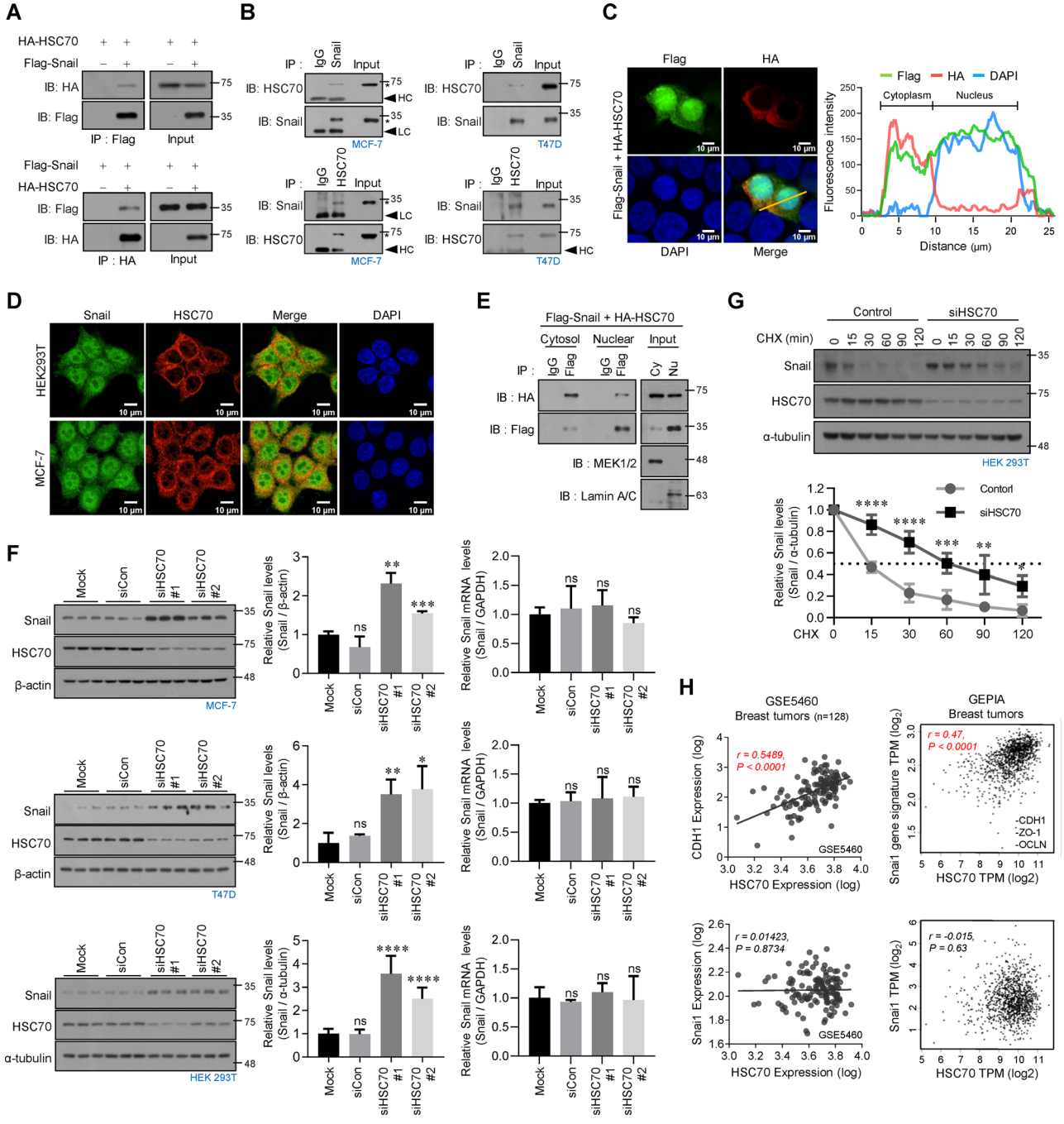

Fig. 1 (See legend on next page.)

(See figure on previous page.)

Fig. 1 HSC70 interacts with Snail in the cytosol and decreases its protein stability. (**A**) Interaction between exogenous HSC70 and Snail. HEK293T cells were transfected with HA-HSC70 and Flag-Snail. Cell lysates were immunoprecipitated with anti-Flag or anti-HA antibodies and analyzed by western blot. The presence of HA-HSC70 was detected using anti-HA antibody (upper panel), and the presence of Flag-Snail was detected using anti-Flag antibody (lower panel). (**B**) Interaction between endogenous HSC70 and Snail. Lysates from MCF-7 and T47D cells were immunoprecipitated with an anti-Snail or anti-HSC70 antibodies and analyzed by western blot. The presence of HSC70 was detected using anti-HSC70 antibody (upper panel), and the presence of Snail was detected using anti-Snail antibody (lower panel). (**C**) Colocalization of exogenous HSC70 with Snail in the cytoplasm. HEK293T cells transfected with HA-HSC70 and Flag-Snail were visualized by confocal microscopy after immunostaining with the indicated antibodies (left). Scale bars, 10 μm. The intensity profiles of the fluorescence signals along the yellow lines indicated in the merge images (right). (**D**) Colocalization of endogenous HSC70 with Snail. HEK293T and MCF-7 cells were visualized by confocal microscopy after immunostaining with the indicated antibodies. Scale bars, 10 μm. (**E**) Interaction between exogenous HSC70 and Snail in the cytoplasm. HEK293T cells transfected with HA-HSC70 and Flag-Snail were fractionated into cytosolic and nuclear fractions. Each fraction was immunoprecipitated with an anti-Flag antibody and analyzed by western blot using anti-HA antibody. MEK1/2: a representative cytosolic marker protein, Lamin A/C: a representative nuclear marker protein. (**F**) Immunoblot analysis in HSC70-depleted MCF-7, T47D or HEK293T cells (left). Relative Snail levels were quantified using ImageJ (middle). *, $P < 0.05$: **, $P < 0.01$: ***, $P < 0.001$: ****, $P < 0.0001$ as determined by *t*-test. Snail mRNA levels were analyzed by qRT-PCR (right), normalized to GAPDH. ns, not significant. (**G**) HSC70-depleted HEK293T cells were treated with CHX (100 μg/ml) for the indicated times before harvest. Cell lysates were immunoblotted with the indicated antibodies (upper), and data quantified using ImageJ (lower). Normalized to α-tubulin. *, $P < 0.05$: **, $P < 0.01$: ***, $P < 0.001$: ****, $P < 0.0001$ as determined by t-test. (**H**) Correlation of HSC70 expression with E-cadherin (CDH1) or Snail expression in published microarray data sets (GSE5460, $n = 128$, left). Scatter plots show the correlation between HSC70 and Snail gene signature (E-cadherin, ZO-1, and Occludin) genes or between HSC70 and Snail gene according to Pearson correlation analysis (GEPIA2, right)

of macroautophagy, induced stabilization of p62, a well-recognized macroautophagy substrate, without affecting Snail levels (Fig. S4A). Further, macroautophagy was specifically inhibited by ATG7 knock down using two siRNAs, which did not affect Snail protein levels in HEK293T and MCF-7 cells (Fig. S4B). These results indicate that lysosomal Snail degradation may occur independent of macroautophagy.

Snail is a novel substrate of CMA

The association of Snail degradation with CMA was assessed [32, 33], by examining the interaction between exogenously expressed LAMP2A and Snail in HEK293T cells (Fig. 3A), which was markedly inhibited by HSC70 depletion (Fig. 3B). While the blockage of CMA activity via LAMP2A depletion elevated Snail levels in HEK293T, MCF-7, and T47D cells, its mRNA levels remained unchanged (Fig. 3C). Downregulation of LAMP2B, an LAMP2 isotype that does not participate in CMA, did not increase Snail levels (Fig. 3D). Further, immunofluorescence analysis revealed that lysosomal localization of Snail was markedly suppressed by LAMP2A depletion (Fig. 3E). In this experiment, all cells were treated with NL because NL treatment inhibits lysosomal degradation and thereby enhances the lysosomal localization of Snail (Fig. 2C). A cycloheximide (CHX) pulse-chase analysis demonstrated that LAMP2A depletion markedly extended the half-life of endogenous Snail (from 10 min to 60 min, Fig. 3F). Database analysis revealed positive correlation of LAMP2A mRNA levels with that of negatively regulated Snail target genes, but not with Snail mRNA levels (Fig. 3G). These results suggest that Snail may be an autophagic substrate that is degraded via CMA. While elevation of Snail levels post LAMP2A depletion was further enhanced by MG132 treatment, it was unaffected by NL treatment (Fig. 3H). Further, Snail ubiquitination was unchanged post LAMP2A depletion (Fig. 3I). These results suggest that LAMP2A may degrade Snail in a lysosome-dependent, but proteasome-independent manner.

The presence of one or several KFERQ-like motifs is critical for a CMA substrate to be recognized by HSC70 and be subsequently degraded [36, 41]. Several KFERQ-like motifs exist in Snail (Fig. S5A), of which the three motifs located within the 40–78 amino acids region that interacts with HSC70 were altered (Fig. S5B). All constructs except the 58AAAA mutant Snail (58AAAA-Snail) protein, where four amino acids starting from position 58 were replaced with alanine interacted with HSC70 (Fig. S5C). Further, 58AAAA-Snail did not interact with LAMP2A (Fig. S5D) and did not demonstrate lysosomal accumulation (Fig. S5E and F). The 58AAAA-Snail was expressed at higher levels than that in wild-type Snail, which showed no further enhancement post NL treatment (Fig. S5G) or LAMP2A depletion (Fig. S5H). Thus, Snail may be a classic CMA substrate that harbors a putative recognition motif within the 58–62 amino acids region.

Evasion of CMA-mediated Snail degradation induces EMT and increases metastatic abilities in luminal-type breast cancer cells

MCF-7 cells expressing Flag-tagged 58AAAA-Snail that avoids CMA-mediated degradation were generated to decipher the role of CMA on Snail function in breast cancer cells. Consistent with results in HEK293T cells (Fig. S5G and H), 58AAAA-Snail expression levels were higher than those of wild-type Snail, and were not enhanced by NL treatment (Fig. 4A) or LAMP2A depletion (Fig. 4B). Further, 58AAAA-Snail half-life was significantly prolonged as compared to that of WT-Snail (from 15 min to 90 min, Fig. 4C). These results suggest that 58AAAA-Snail was not degraded by CMA in breast cancer cells, and was more stable than WT-Snail.

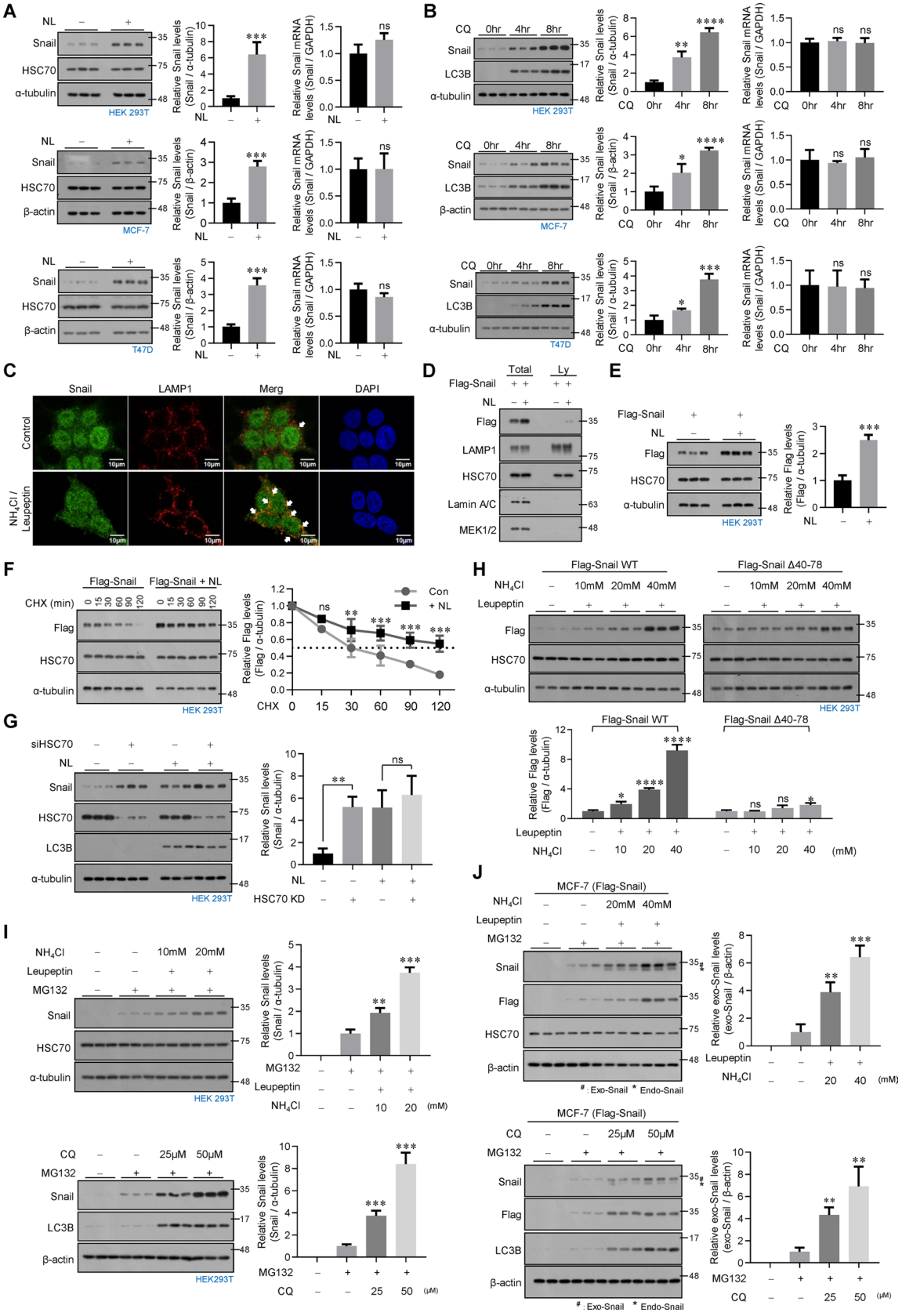

Fig. 2 (See legend on next page.)

(See figure on previous page.)

Fig. 2 HSC70 induces Snail protein degradation through lysosome. (**A**, **B**) Immunoblot analysis in ammonium chloride and leupeptin (NL)-treated (**A**) or chloroquine (CQ)-treated (**B**) HEK293T, MCF-7, or T47D cells (left). Relative Snail levels were quantified using ImageJ (middle). ***, $P < 0.001$ as determined by *t*-test. Snail mRNA levels were analyzed by qRT-PCR (right), normalized to GAPDH. ns, not significant. (**C**) Colocalization of Snail with LAMP1. HEK293T cells treated with or without NL were visualized by confocal microscopy after immunostaining with the indicated antibodies. Scale bars, 10 μm. (**D**) Snail accumulation in lysosomes. HEK293T cells transfected with Flag-Snail and treated with NL. Lysosome lysates were immunoblotted with indicated antibodies. (**E**) HEK293T cells transfected with Flag-Snail were treated with NL. Cell lysates were immunoblotted with the indicated antibodies (left). Relative Snail (Flag) levels were quantified using ImageJ (right). ***, $P < 0.001$ as determined by t-test. (**F**) HEK293T cells transfected with Flag-Snail and treated with NL were subjected to CHX treatment (100 μg/ml) for the indicated times before harvest. Cell lysates were immunoblotted with the indicated antibodies (left), and data quantified using ImageJ (right). Normalized to α-tubulin. **, $P < 0.01$: ***, $P < 0.001$ as determined by t-test. ns, not significant. (**G**) HSC70-depleted HEK293T cells were treated with NL. Cell lysates were immunoblotted with the indicated antibodies (left). Relative Snail levels were quantified using ImageJ (right). **, $P < 0.01$ as determined by t-test. ns, not significant. (**H**) HEK293T cells transfected with Flag-Snail WT or Flag-Snail-Δ40–78 were treated with NL. Cell lysates were immunoblotted with the indicated antibodies (upper). Relative Snail (Flag) levels were quantified using ImageJ (right). *, $P < 0.05$: ****, $P < 0.0001$ as determined by t-test. ns, not significant. (**I**) Immunoblot analysis in NL (upper left) or CQ (lower left) and/or MG132-treated HEK293T cells. Relative Snail levels were quantified using ImageJ (right). **, $P < 0.01$: ***, $P < 0.001$ as determined by *t*-test. (**J**) Immunoblot analysis in NL (upper left) or CQ (lower left) and/or MG132-treated Flag-Snail-expressing MCF-7 cells. Relative Snail levels were quantified using ImageJ (right). **, $P < 0.01$: ***, $P < 0.001$ as determined by *t*-test. #, exogenously expressed Snail. *, endogenously expressed Snail

Among the three stable MCF-7 cell lines expressing Flag-tag (Con), WT-Snail, or 58AAAA-Snail, the morphology of the 58AAAA-Snail-expressing cells was distinct from that of the control and WT-Snail-expressing cells. While confocal microscopy of phalloidin-stained cells confirmed the presence of filopodia, lamellipodia, and microspikes in 58AAAA-Snail-expressing MCF-7 cells, the control and WT-Snail-expressing cells exhibited lesser staining and cellular protrusions (Fig. 4D). This led us to measure expression levels of EMT marker genes in these cells. As expected, while WT-Snail expression only affected the expression of various EMT marker proteins marginally, the effect was substantially enhanced by 58AAAA-Snail expression (Fig. 4E). Further, while LAMP2A depletion in WT-Snail-expressing MCF-7 cells reduced the expression of epithelial marker proteins, such as E-cadherin and Occludin, no significant changes were evident in 58AAAA-Snail-expressing cells (Fig. S6A). These results suggest that evasion of CMA-mediated Snail degradation may contribute to EMT induction in luminal-type breast cancer cells. An investigation into the potential alteration of the migratory properties of MCF-7 cells by Snail using a wound-healing assay revealed that a larger number of WT-Snail-expressing MCF-7 cells migrated into the scratch wound in 24 h as compared to that in the control cells, and the effect was further enhanced in 58AAAA-Snail expressing cells (Fig. 4F). Similar results regarding the migratory ability of 58AAAA-Snail-expressing cells, WT-Snail-expressing MCF-7 cells, and control cells was evident in the in vitro invasion assay (Fig. 4G). While LAMP2A depletion in WT-Snail-expressing MCF-7 cells increased migration and invasion abilities, no further enhancement was evident in 58AAAA-Snail-expressing cells (Fig. S6B and C). Additionally, all three cell types demonstrated similar growth rates under similar growth conditions (Fig. 4H), indicating that enhanced migration and invasion abilities of WT-Snail- and 58AAAA-Snail-expressing cells are independent of growth rate. Further, lung metastasis of 58AAAA-Snail-expressing MCF-7 cells was observed to be significantly higher than that of WT-Snail-expressing or control cells, post injection of WT-Snail-, 58AAAA-Snail-expressing MCF-7 cells, or control cells into the tail vein of nude mice (Fig. 4I). These findings indicate that evasion of CMA-mediated Snail degradation may induce EMT and increase metastatic abilities in luminal-type breast cancer cells.

Serum starvation induces Snail degradation by CMA in TNBC cells

We demonstrated high expression levels of Snail in TNBC cell lines as compared to that in luminal-type breast cancer cell lines (Fig. S1A), and its putative role as a substrate for CMA in luminal-type of breast cancer cells. The effect of serum starvation, which activates CMA via elevated LAMP2A expression on Snail in TNBC cells was assessed [42, 43]. Serum starvation increased LAMP2A expression in MDA-MB-231 and BT549 cells, and concomitantly decreased Snail protein levels without influencing its mRNA levels (Fig. 5A). LAMP2A depletion or treatment with NL or CQ inhibited serum starvation-mediated downregulation of Snail, which was not inhibited by 3-MA (Fig. 5B and Fig. S7). The expression of epithelial marker proteins such as Occludin and Claudin 1 was also increased by serum starvation, but LAMP2A depletion suppressed this (Fig. S8). These results suggest that serum starvation may inhibit EMT in TNBC cell lines by inducing CMA-mediated Snail degradation.

Ectopic LAMP2A expression alone was unable to reduce Snail expression in MDA-MB-231 and BT549 cells to the same extent as that caused by serum starvation (Fig. 5C). Further, while LAMP2A depletion markedly increased Snail levels in luminal-type breast cancer cell lines, the effect was marginal in TNBC cell lines (Fig. 5D). These results indicate that apart from increased LAMP2A expression, other conditions must be met to ensure decreased Snail expression in TNBC cells post serum starvation. Snail predominantly localized to

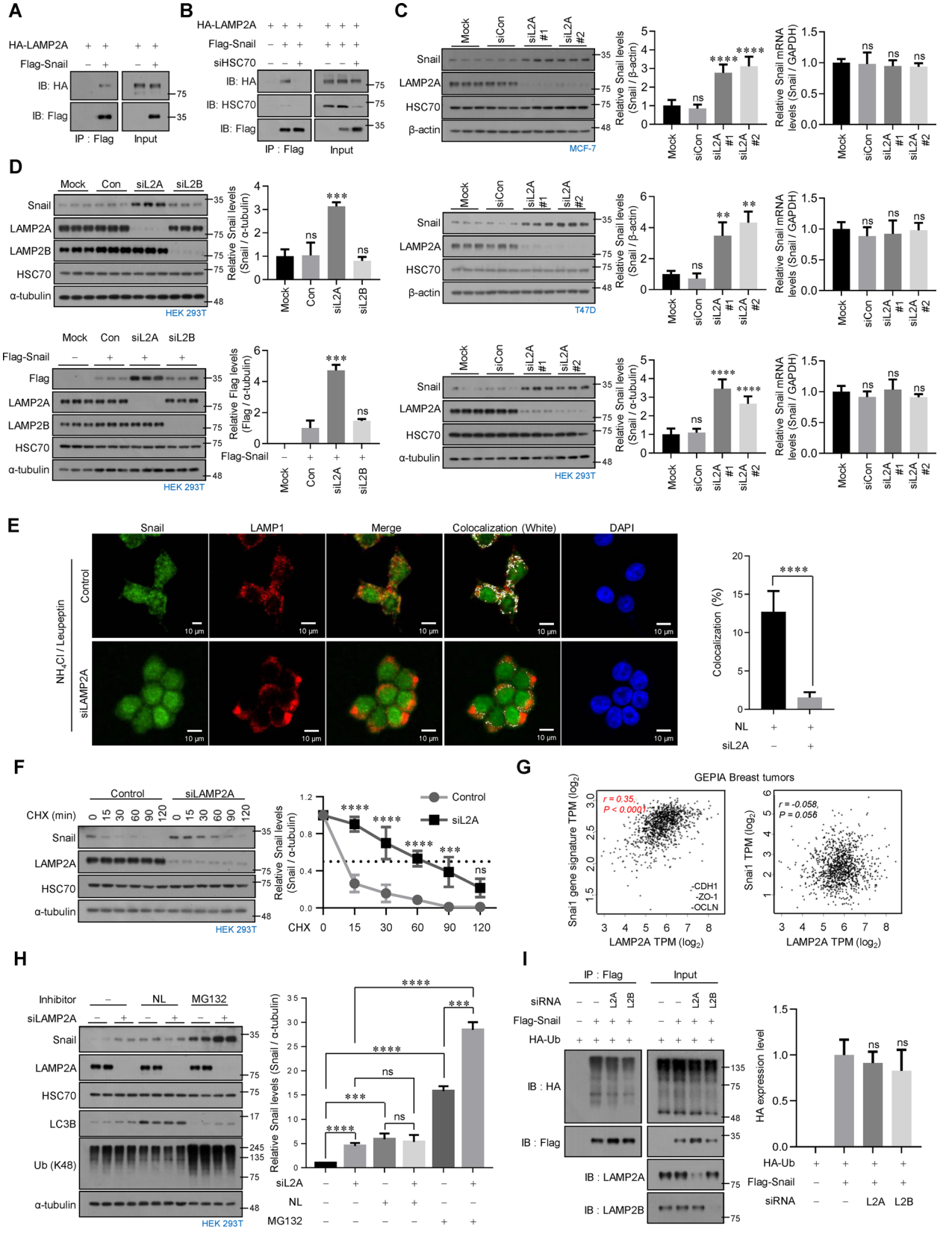

Fig. 3 (See legend on next page.)

(See figure on previous page.)

Fig. 3 Snail is a novel substrate of CMA. (**A**) Interaction between exogenous LAMP2A and Snail. HEK293T cells transfected with HA-LAMP2A and Flag-Snail were immunoprecipitated with an anti-Flag antibody and analyzed by western blot using anti-HA antibody. (**B**) Interaction between exogenous LAMP2A and Snail in the absence of HSC70. HEK293T cells transfected with HA-LAMP2A and Flag-Snail were depleted of HSC70. Cell lysates were immunoprecipitated with an anti-Flag antibody and analyzed by western blot using anti-HA antibody. (**C**) Immunoblot analysis in LAMP2A-depleted MCF-7, T47D or HEK293T cells (left). Relative Snail levels were quantified using ImageJ (middle). **, $P<0.01$: ****, $P<0.0001$ as determined by *t*-test. Snail mRNA levels were analyzed by qRT-PCR (right), normalized to GAPDH. ns, not significant. (**D**) Immunoblot analysis in LAMP2A or LAMP2B-depleted HEK293T cells (left). Relative Snail levels were quantified using ImageJ (right). ***, $P<0.001$ as determined by *t*-test. ns, not significant. (**E**) Colocalization of Snail with LAMP1 in LAMP2A-depleted HEK293T cells. Control or LAMP2A-depleted HEK293T cells treated with NL were visualized by confocal microscopy after immunostaining with the indicated antibodies. Scale bars, 10 μm. (**F**) LAMP2A-depleted HEK293T cells were treated with CHX (100 μg/ml) for the indicated times before harvest. Cell lysates were immunoblotted with the indicated antibodies (left), and data quantified using ImageJ (right). Normalized to α-tubulin. ***, $P<0.001$: ****, $P<0.0001$ as determined by t-test. ns, not significant. (**G**) Scatter plots show the correlation between LAMP2A and Snail gene signature (E-cadherin, ZO-1, and Occludin) genes or between LAMP2A and Snail gene according to Pearson correlation analysis (GEPIA2). (**H**) LAMP2A-depleted HEK293T cells were treated with NL or MG132. Cell lysates were immunoblotted with the indicated antibodies (left). Relative Snail levels were quantified using ImageJ (right). ***, $P<0.001$: ****, $P<0.0001$ as determined by t-test. ns, not significant. (**I**) LAMP2A or LAMP2B-depleted HEK293T cells transfected with Flag-Snail and HA-ubiquitin were treated with MG132. Cell lysates were immunoprecipitated with an anti-Flag antibody and analyzed by immunoblot using anti-HA antibody

the nucleus in TNBC cells, unlike luminal-type breast cancer cells (Fig. S9). Immunofluorescence co-staining of Snail and LAMP1 in MDA-MB-231 cells revealed nuclear localized Snail under normal conditions that translocated to the cytoplasm and localized to lysosomes during serum starvation (Fig. 5E). Fractionation analysis revealed a decrease in nuclear, and an increase in cytoplasmic Snail levels during serum starvation (Fig. 5F). Further, while nuclear Snail levels post NL treatment during serum starvation were unchanged, cytoplasmic levels were further increased (Fig. 5F). Treatment with Leptomycin B (LMB), a CRM1-dependent Snail nuclear export inhibitor [16, 44], suppressed serum starvation induced decrease of Snail expression in MDA-MB-231 and BT549 cells (Fig. 5G). These results suggest that cytoplasmic translocation of Snail is essential for its degradation in serum starved TNBC cells.

The subcellular localization of Snail protein could be determined by several kinases, including GSK3β, PKD1, PAK1, and Akt [15, 27, 45, 46]. As shown in Fig. 5H, serum starvation significantly increased GSK3β and PKD1 activities, which can induce the cytoplasmic translocation of Snail [15, 45], and decreased the expression of PAK1 and Akt activity, which enables the nuclear retention of Snail [27, 46]. These results suggest that serum starvation in TNBC cells may not only increase LAMP2A expression, but also activate signal transduction pathways essential for the nuclear to cytoplasmic translocation of Snail prior to its degradation by CMA.

Nuclear to cytoplasmic translocation of Snail is prerequisite for CMA-mediated degradation in luminal-type breast cancer cells

Snail protein translated in the cytoplasm is targeted to the nucleus by its nuclear localization signal (NLS) [47, 48]. Our results indicate that in TNBC cells, Snail localizes to the nucleus, where it carries out its functions while evading CMA. Conversely, in luminal-type breast cancer cells, Snail translocates to the cytoplasm, where it undergoes degradation via CMA. While LMB treatment significantly increased Snail levels in MCF-7 cells, the effect was minimal in MDA-MB-231 cells (Fig. 6A). LMB-treated MCF-7 cells demonstrated complete nuclear localization of cytoplasmic Snail (Fig. 6B). Additionally, MDA-MB-231 cells that received the same treatment continued to retain Snail within the nucleus (Fig. 6B). While LAMP2A depletion increased Snail levels in HEK293T and MCF-7 cells, the same was not enhanced further by LMB treatment (Fig. 6C). Further, LAMP2A depletion led to higher cytoplasmic Snail levels than that in the nucleus, which was countered by LMB treatment (Fig. 6D). The interaction and colocalization of Snail and HSC70 were also significantly inhibited by LMB treatment (Fig. 6E and F). These results suggest that nuclear to cytoplasmic Snail translocation in luminal-type breast cancer cells is essential for its degradation via CMA.

TGF-β induces EMT by increasing Snail expression in a variety of cells [49]. MCF-7 cells were treated with TGF-β to determine the role of CMA-mediated Snail degradation during TGF-β-induced EMT in luminal-type breast cancer cells. TGF-β increased Snail expression and decreased E-cadherin expression in MCF-7 cells (Fig. 6G). However, the expression of LAMP2A and HSC0, key mediators of CMA, was not changed by TGF-β treatment (Fig. 6G). To further clarify the role of TGF-β in CMA regulation, we examined the expression levels of other known CMA substrates, including PKM2, Histone H3, HK2, and IκBα [50–53]. Our analysis revealed that the expression of these substrates remained unchanged upon TGF-β treatment (Fig. 6G), indicating that TGF-β does not inhibit CMA activity in MCF-7 cells. In addition, in MCF-7 cells, TGF-β significantly reduced the interaction of Snail with HSC70 (Fig. 6H), induced its nuclear localization and reduced its lysosomal localization (Fig. 6I). Further, while TGF-β increased WT-Snail expression in MCF-7 cells, the elevated 58AAAA-Snail expression was unchanged (Fig. 6J). Taken together,

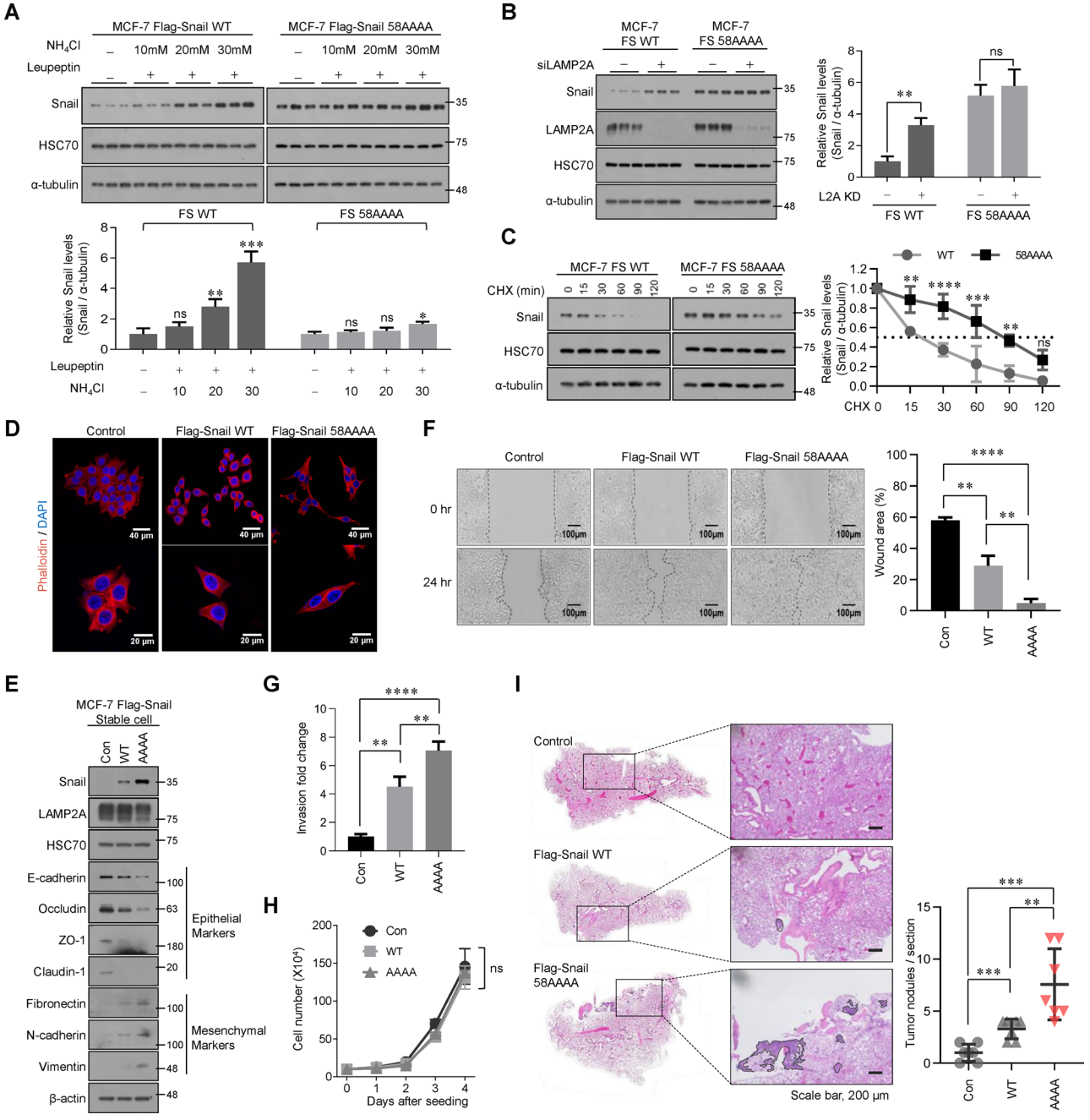

Fig. 4 (See legend on next page.)

(See figure on previous page.)

Fig. 4 Evasion of CMA-mediated Snail degradation induces EMT and increases metastatic abilities in luminal-type breast cancer cells. (**A**) Immunoblot analysis of NL-treated WT-Snail- or 58AAAA-Snail-expressing MCF-7 cells (upper). Relative Snail levels were quantified using ImageJ (lower). *, $P<0.05$: **, $P<0.01$: ***, $P<0.001$ as determined by *t*-test. ns, not significant. (**B**) Immunoblot analysis in LAMP2A-depleted WT-Snail- or 58AAAA-Snail-expressing MCF-7 cells (left). Relative Snail levels were quantified using ImageJ (right). **, $P<0.01$ as determined by *t*-test. ns, not significant. (**C**) WT-Snail or 58AAAA-Snail-expressing MCF-7 cells were treated with CHX (100 μg/ml) for the indicated times before harvest. Cell lysates were immunoblotted with the indicated antibodies (left), and data quantified using ImageJ (right). Normalized to α-tubulin. **, $P<0.01$: ***, $P<0.001$: ****, $P<0.0001$ as determined by t-test. ns, not significant. (**D**) Morphological changes of WT-Snail or 58AAAA-Snail-expressing MCF-7 cells. WT-Snail-, 58AAAA-Snail-expressing MCF-7 and control cells were stained with TRITC-conjugated phalloidin and visualized by confocal microscopy. Scale bars, 40 μm–20 μm. (**E**) Expression levels of EMT marker proteins in WT-Snail-, 58AAAA-Snail-expressing MCF-7 and control cells were analyzed by immunoblotting. (**F**) WT-Snail, 58AAAA-Snail-expressing MCF-7 and control cells were analyzed in wound-healing assays by visualizing wound closure via phase-contrast microcopy (left). Wound areas were measured using WimScratch software (Wimasis). The data shown represent the percentage of the wound area and are expressed as the means ± SD of three individual experiments (right). **, $P<0.01$: ****, $P<0.0001$ as determined by *t*-test. (**G**) WT-Snail-, 58AAAA-Snail-expressing MCF-7 and control cells were seeded onto Matrigel matrix-coated top chambers, and the fold-changes of invading cells were measured after 30 h. The data shown are expressed as the means ± SD of three individual experiments, each performed in triplicate. **, $P<0.01$: ****, $P<0.0001$ as determined by *t*-test. (**H**) The indicated cells were seeded in a 6-well plate at a concentration of 1×10^5 cells per well. After incubation for 1 to 4 days, the viable cells were counted with a hemocytometer after trypan blue staining. **(I)** About 2×10^6 of the MCF-7 cells stably expressing WT-Snail, 58AAAA-Snail, or control cells were injected into the nude mice by tail-vein injection. Representative pictures of HE staining of lung sections (left). Scale bars, 200 μm. The number of metastatic lung nodules in individual mice was quantified at 6 weeks after tail-vein injection (right). The data are shown as the means ± SD of 7 mice/group. **, $P<0.01$: ***, $P<0.001$ as determined by *t*-test

our results suggest that in luminal-type breast cancer cells, TGF-β does not directly decrease CMA activity, but rather induces nuclear translocation of the Snail to inhibit CMA-mediated degradation, which leads to EMT induction.

Expression of HSC70 correlates with the expression of Snail target genes in patients with luminal-type breast cancer

HSC70 mRNA levels in breast cancer patients correlates positively with E-cadherin expression, but not with Snail mRNA levels (Fig. 1H). On stratification into luminal-type breast cancer and TNBC patients, the former exhibited positive correlation of HSC70 with E-cadherin levels, and negative correlation with Vimentin levels. No such significant correlations were evident in TNBC patients (Fig. 7A and Fig. S10A). Additionally, patients with both types of breast cancer exhibited no correlation between HSC70 and the mRNA levels of EMT-related transcription factors (Fig. 7B and Fig. S10B). The Kaplan–Meier analysis revealed that high expression of HSC70 was associated with significantly increased relapse free survival (RFS) in patients with luminal-type breast cancer, but there was little correlation in patients with TNBC (Fig. 7C).

Discussion

Our results support a novel role for CMA in the regulation of intracellular Snail levels, which is determined by the subcellular localization of Snail protein. We demonstrate CMA-mediated cytosolic Snail degradation that is independent of proteasome, in luminal-type breast cancer cells with low Snail levels. We further show that in TNBC cells, unlike luminal-type breast cancer cells, Snail localizes to the nucleus, which prevents its degradation by CMA (Fig. 7C). Our findings identify CMA as a novel pathway for cytosolic Snail degradation, and provide evidence in support of high stability of nuclear Snail.

CMA plays a dual role in cancer, which adds complexity to its function in cellular processes. On one hand, in normal cells, CMA contributes to tumor suppression by selectively degrading oncogenic proteins such as HK2, MDM2, MYC, and Eps8, thereby preventing tumor development [52, 54–56]. A reduction in CMA activity has been associated with malignant transformation and tumorigenesis. On the other hand, CMA is often upregulated in various cancer types [57], where it may support tumor progression by enhancing cellular proliferation and increasing tumorigenic capacity. This is achieved through mechanisms such as protection against oxidative damage, removal of negative regulators of cell proliferation, and maintenance of metabolic states that favor cancer growth [50, 58–61]. Although our study does not directly focus on the role of CMA in cancer progression, these findings highlight the importance of understanding the diverse functions of CMA, as they may have broader implications for the pathological processes investigated in our research.

Blocking LAMP2A in the CMA pathway significantly reduces metastatic ability of lung cancer cells [57], and inhibition of CMA activity in colorectal cancer decreases tumor metastasis and promotes drug sensitivity [62]. Further, CMA promotes breast cancer cell metastasis by downregulating ATG5-dependent macroautophagy [63]. However, we found that Snail, a key EMT regulator, is degraded via CMA in luminal-type breast cancer cells, but evades CMA in TNBC cells. The 58–62 amino acids region (58-MLIWD-62) of Snail enables its interaction with HSC70, and subsequent lysosomal translocation via LAMP2A for degradation. We also demonstrated that Snail containing a modified HSC70 binding motif avoided CMA-mediated degradation, induced EMT, and promoted metastasis in luminal-type breast cancer cells. In concurrence with our results, CMA regulates degradation of metastasis promoting proteins, such as HIF-1α

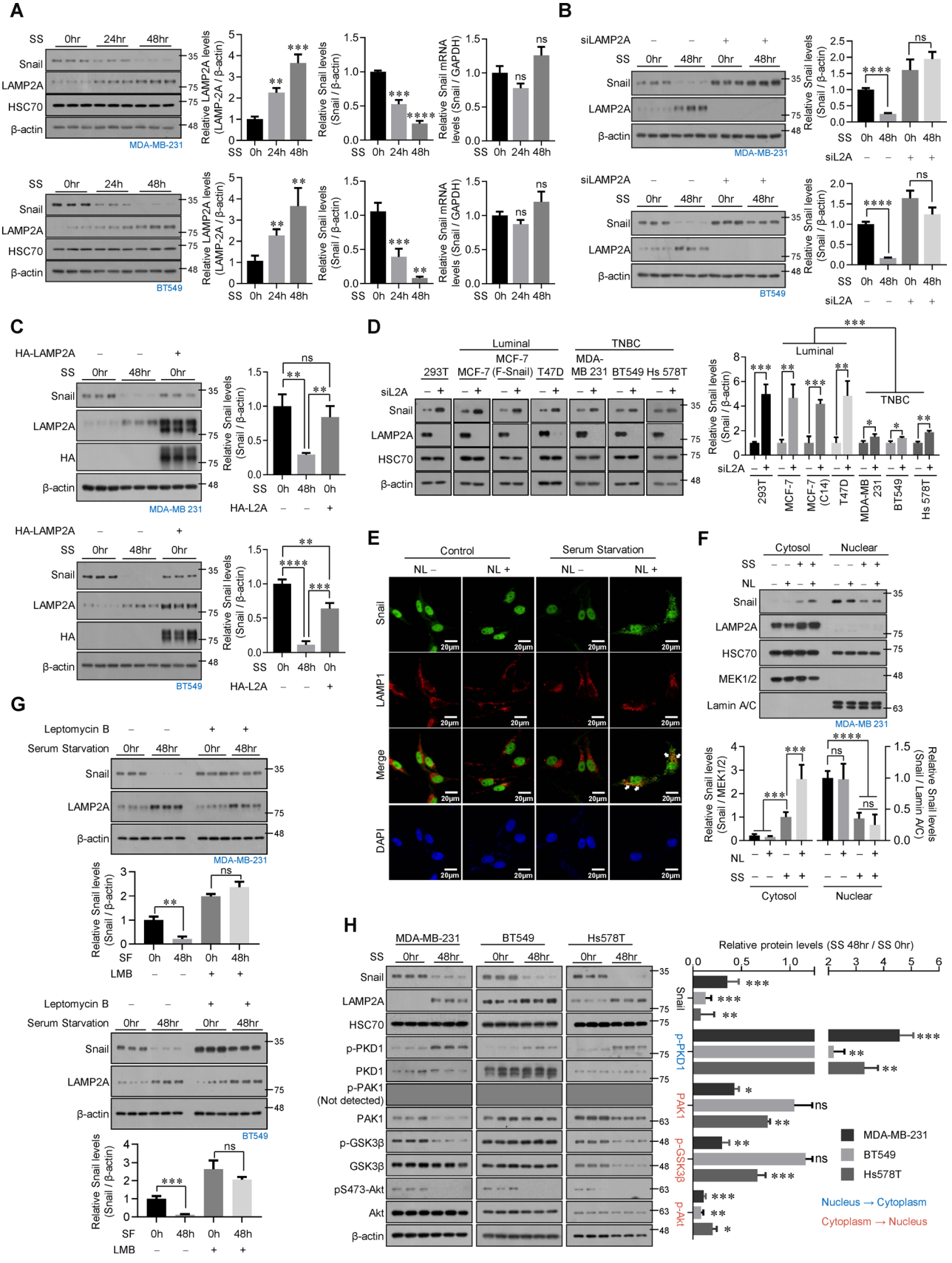

Fig. 5 (See legend on next page.)

(See figure on previous page.)

Fig. 5 Serum starvation induces Snail degradation by CMA in TNBC cells. (**A**) Immunoblot analysis of serum-starved MDA-MB-231 or BT549 cells (left). Relative LAMP2A and Snail levels were quantified using ImageJ (middle). **, $P < 0.01$: ***, $P < 0.001$: ****, $P < 0.0001$ as determined by *t*-test. Snail mRNA levels were analyzed by qRT-PCR (right), normalized to GAPDH. ns, not significant. (**B**) LAMP2A-depleted MDA-MB-231 or BT549 cells were serum starved. Cell lysates were immunoblotted with the indicated antibodies (left). Relative Snail levels were quantified using ImageJ (right). ****, $P < 0.0001$ as determined by t-test. ns, not significant. (**C**) MDA-MB-231 or BT549 cells transfected with LAMP2A were immunoblotted with the indicated antibodies (left). Relative Snail levels were quantified using ImageJ (right). **, $P < 0.01$: ***, $P < 0.001$: ****, $P < 0.0001$ as determined by *t*-test. ns, not significant. (**D**) Immunoblot analysis in LAMP2A-depleted luminal-type breast cancer cells or TNBC cells (left). Relative Snail levels were quantified using ImageJ (right). *, $P < 0.05$: **, $P < 0.01$: ***, $P < 0.001$ as determined by *t*-test. (**E**) Colocalization of Snail with LAMP1 upon NL treatment in serum-starved MDA-MB-231 cells. MDA-MB-231 cells treated with NL under serum starvation were visualized by confocal microscopy after immunostaining with the indicated antibodies. Scale bars, 20 μm. (**F**) Serum starved MDA-MB-231 cells were treated with NL. Cytosolic and nuclear fractions were immunoblotted with the indicated antibodies (upper). Relative Snail levels were quantified using ImageJ software (lower). ***, $P < 0.001$: ****, $P < 0.0001$ as determined by *t*-test. ns, not significant. (**G**) Immunoblot analysis of serum-starved MDA-MB-231 or BT549 cells treated with or without Leptomycin B (upper). Relative Snail levels were quantified using ImageJ software (lower). **, $P < 0.01$: ***, $P < 0.001$ as determined by *t*-test. ns, not significant. (**H**) Immunoblot analysis of serum-starved MDA-MB-231, BT549 or Hs578T cells (left). Relative Snail, p-PKD1, PAK1, p-GSK3β (inactive form) and p-Akt levels were quantified using ImageJ (right). *, $P < 0.05$: **, $P < 0.01$: ***, $P < 0.001$ as determined by *t*-test

and p65 [64, 65]. While CMA targets p65, the protein is stabilized by reduced CMA activity during EMT, resulting in increased metastatic capacity of cancer cells [65].

The differential expression levels of WT-Snail and the 58AAAA-Snail mutant significantly impact their respective abilities to induce EMT and metastatic phenotypes. Our findings indicate that WT-Snail is subject to CMA-mediated degradation, leading to lower expression levels, whereas the 58AAAA-Snail mutant evades this degradation pathway, resulting in higher expression levels and more pronounced EMT and metastatic behaviors. This was further corroborated by experiments in which LAMP2A knockdown equalized the expression levels of WT-Snail and 58AAAA-Snail, leading to similar EMT, migration, and invasion phenotypes. These observations underscore the critical role of CMA in regulating Snail stability and its downstream effects on EMT. The rapid turnover of WT-Snail via CMA likely contributes to its reduced impact on EMT compared to the more stable 58AAAA-Snail mutant. Therefore, the elevated EMT and metastatic capabilities observed in 58AAAA-Snail expressing cells can be attributed to its increased expression levels due to evasion of CMA-mediated degradation.

Snail retains its nuclear localization and avoids CMA in TNBC cells, but not in luminal-type breast cancer cells. During starvation, Snail translocates to the cytoplasm and undergoes CMA. The subcellular localization of Snail is regulated by several kinases, with phosphorylation by GSK3β and PKD1 promoting its nuclear export and degradation, and that by PAK1 and Akt retaining its nuclear localization and stability [15, 27, 45, 46]. Our results suggest that kinase activities involved in cytoplasmic Snail translocation are low, and those involved in retaining it within the nucleus are high in TNBC cells, which enables avoidance of cytoplasmic Snail degradation.

To the best of our knowledge, this study is the first to provide evidence of CMA-mediated Snail degradation, which may explain its greater nuclear stability than that in the cytoplasm, and its higher expression in TNBC cells than in luminal-type breast cancer cells. We identify CMA as a critical regulator of Snail stability, with distinct mechanisms in different breast cancer subtypes. This novel regulatory pathway offers promising avenues for therapeutic interventions via modulating Snail levels to prevent breast cancer progression and metastasis. Future research on the elucidation of the molecular mechanisms underlying the nuclear export of Snail, and the specific modulation of CMA activity, will aid development of targeted therapies against aggressive breast cancer subtypes.

While our in vitro findings demonstrate that starvation induces Snail degradation through CMA and represses EMT in TNBC cells, in vivo validation is essential to confirm these results. Future studies will focus on performing in vivo experiments to substantiate the role of starvation-induced CMA in regulating Snail degradation and EMT in TNBC.

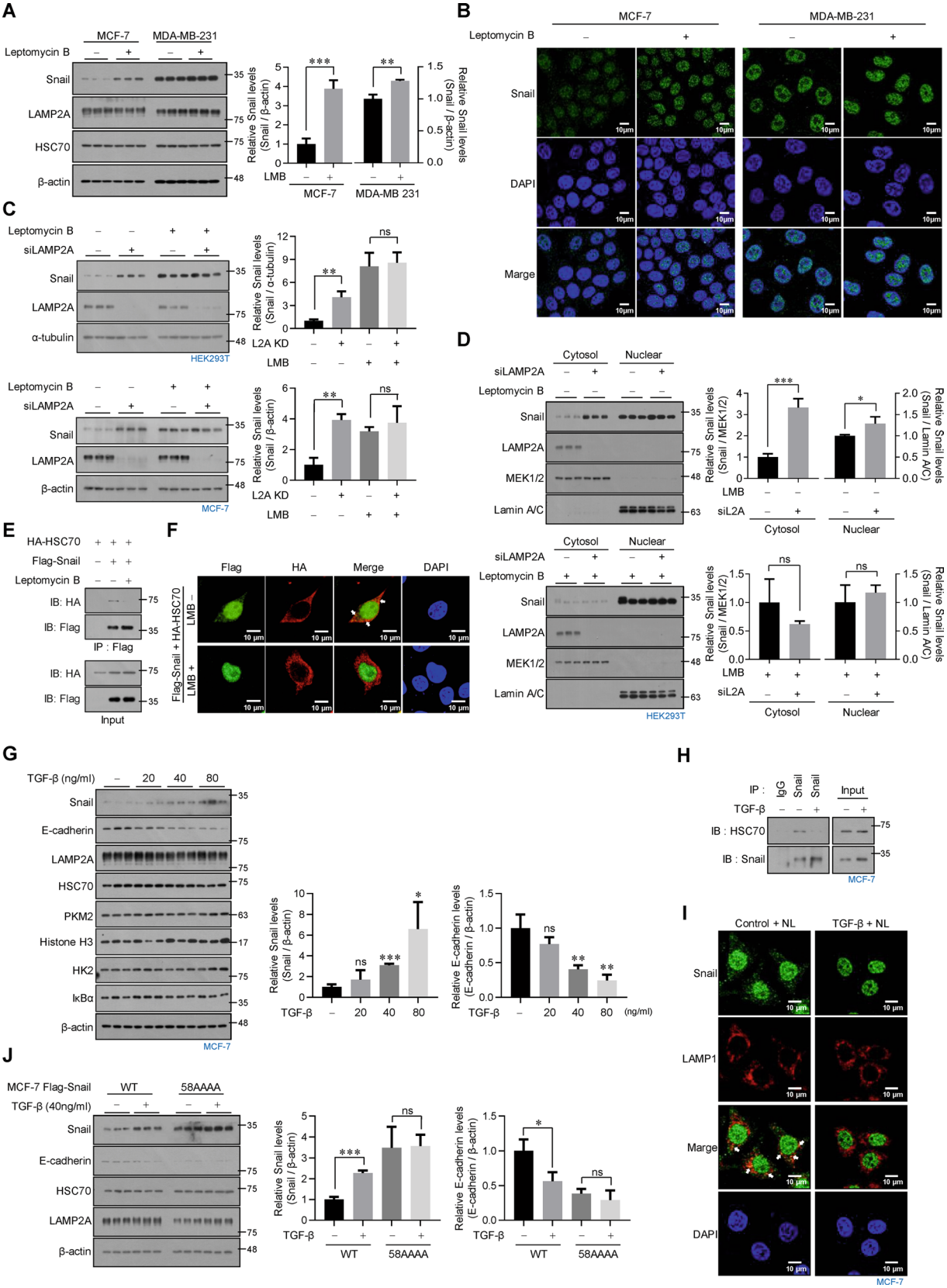

Fig. 6 (See legend on next page.)

(See figure on previous page.)

Fig. 6 Nuclear to cytoplasmic translocation of Snail is prerequisite for CMA-mediated degradation in luminal-type breast cancer cells. (**A**) Immunoblot analysis of Leptomycin B-treated MCF-7 or MDA-MB-231 cells (left). Relative Snail levels were quantified using ImageJ (middle). **, $P < 0.01$: ***, $P < 0.001$: ****, $P < 0.0001$ as determined by *t*-test. (**B**) Subcellular localization of endogenous Snail protein in Leptomycin B-treated MCF-7 or MDA-MB-231 cells. MCF-7 or MDA-MB-231 cells treated with or without Leptomycin B were visualized by confocal microscopy after immunostaining with the indicated antibodies. Scale bars, 10 μm. (**C**) Immunoblot analysis of LAMP2A-depleted HEK293T or MCF-7 cells treated with or without Leptomycin B (upper). Relative Snail levels were quantified using ImageJ (lower). **, $P < 0.01$ as determined by *t*-test. ns, not significant. (**D**) LAMP2A-depleted HEK293T cells were treated or without Leptomycin B. Cytosolic and nuclear fractions were immunoblotted with the indicated antibodies (left). Relative Snail levels were quantified using ImageJ (right). *, $P < 0.05$: ***, $P < 0.001$ as determined by *t*-test. ns, not significant. (**E**) Interaction between exogenous HSC70 and Snail with or without Leptomycin B treatment. HEK293T cells transfected with HA-HSC70 and Flag-Snail were treated with or without Leptomycin B. Cell lysates were immunoprecipitated with an anti-Flag antibody and analyzed by western blot using anti-HA antibody. (**F**) Colocalization of exogenous HSC70 with Snail with or without Leptomycin B treatment. HA-HSC70 and Flag-Snail were transfected into HEK293T cells, and treated or not with Leptomycin B. HEK293T cells were visualized by confocal microscopy after immunostaining with the indicated antibodies. Scale bars, 10 μm. (**G**) Immunoblot analysis of TGF-β-treated MCF-7 cells (left). Relative Snail and E-cadherin levels were quantified using ImageJ (right). *, $P < 0.05$: **, $P < 0.01$: ***, $P < 0.001$ as determined by *t*-test. ns, not significant. (**H**) Interaction between endogenous HSC70 and Snail with or without TGF-β treatment. MCF-7 cells treated with or without TGF-β were immunoprecipitated with an anti-Snail antibody and analyzed by western blot using anti-HSC70 antibody. (**I**) Colocalization of Snail with LAMP1 after NL treatment in MCF-7 cells treated with or without TGF-β. MCF-7 cells were visualized by confocal microscopy after immunostaining with the indicated antibodies. Scale bars, 10 μm. (**J**) Immunoblot analysis of TGF-β-treated WT-Snail or 58AAAA-Snail-expressing MCF-7 cells (left). Relative Snail and E-cadherin levels were quantified using ImageJ (right). *, $P < 0.05$: ***, $P < 0.001$ as determined by *t*-test. ns, not significant

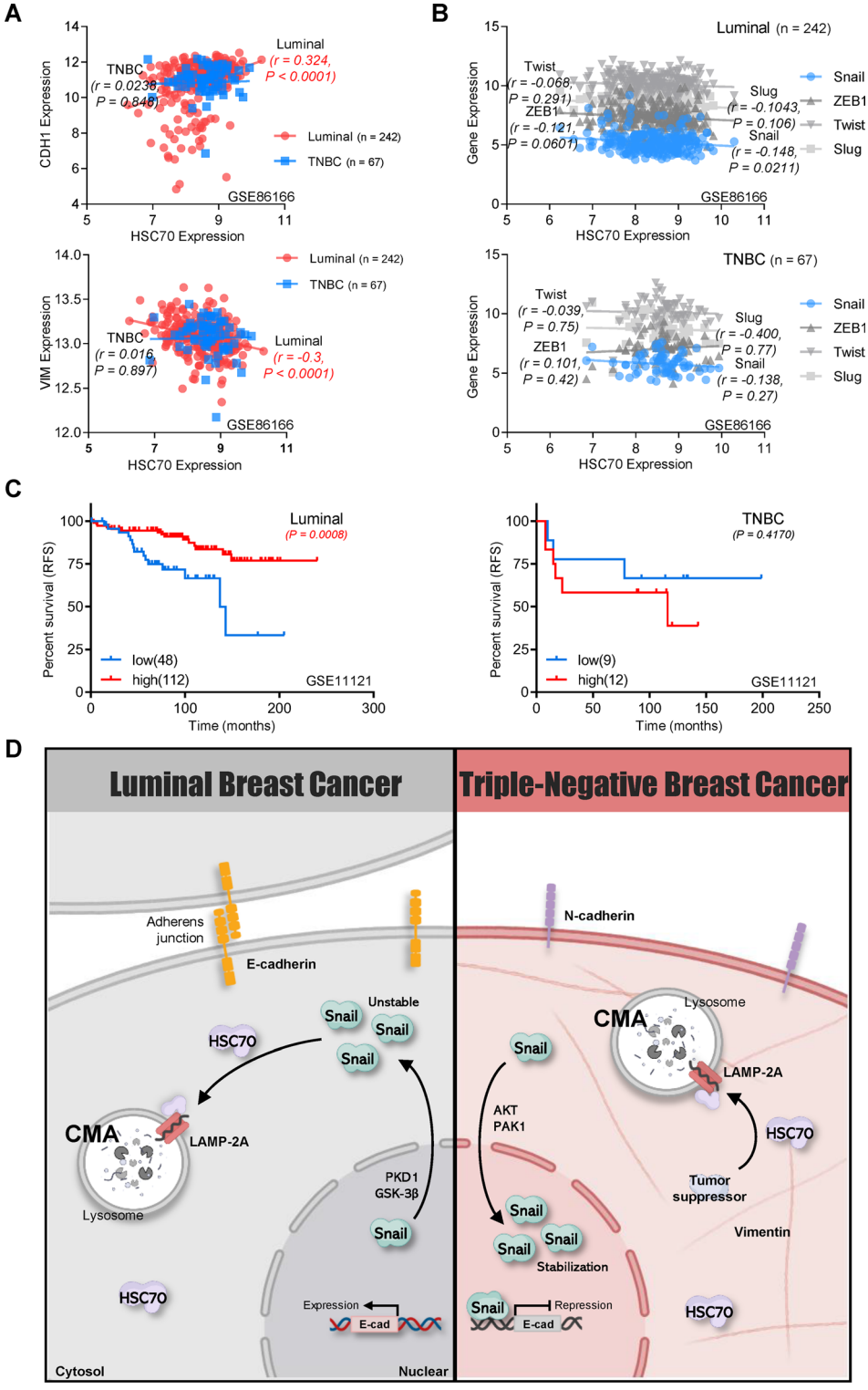

Fig. 7 Expression of HSC70 correlates with the expression of Snail target genes in patients with luminal-type breast cancer. (**A**) Correlation of HSC70 expression with E-cadherin (CDH1) or Vimentin (VIM) expression in breast cancer patients (GSE86166, luminal-type breast cancer patients, $n = 242$; TNBC patients, $n = 67$). (**B**) Correlation of HSC70 expression with the expression of EMT-related transcription factors in breast cancer patients (GSE86166, luminal-type breast cancer patients, $n = 242$; TNBC patients, $n = 67$). (**C**) Association of HSC70 expression with Relapse Free Survival (RFS) in patients with breast cancer. Kaplan-Meier plot showing HSC70 expression and prognosis in breast cancer patients (GSE11121, luminal-type breast cancer patients, $n = 160$; TNBC patients, $n = 21$). Statistical analysis was performed using log-rank tests. (**D**) Schematic diagram showing how CMA modulates Snail protein stability in breast cancer. In luminal-type breast cancer cells, Snail is predominantly localized in the cytoplasm and is susceptible to degradation by CMA, thereby inhibiting EMT. In TNBC cells, Snail remains in the nucleus, escaping CMA-mediated degradation, and promoting EMT

Conclusions

In this study, we identify a novel role of chaperone-mediated autophagy (CMA) for Snail degradation, significant in breast cancer. CMA prevents Snail accumulation in luminal-type breast cancer cells, but Snail evades CMA in TNBC cells. CMA activation reduces Snail in TNBC cells, highlighting its potential as a therapeutic target for breast cancer treatment.

Abbreviations

3-MA	3-methyladenine
β-TrCP1	β-transducin repeat containing E3 ubiquitin protein ligase
CHIP	Carboxy terminus of Hsp70-interacting protein
CHX	Cycloheximide
CMA	Chaperone-mediated autophagy
CQ	Chloroquine
CRM1	Chromosome region maintenance 1
EMT	Epithelial–mesenchymal transition
GSK-3β	Glycogen synthase kinase-3β
HSC70	Heat shock cognate protein 70
LAMP2A	Lysosome-associated membrane protein type 2 A
LMB	Leptomycin B
NES	Nuclear export sequence
NL	Ammonium chloride and leupeptin
NLS	Nuclear localization signal
PAK1	p21 (RAC1) activated kinase 1
PKD1	Polycystic Kidney Disease 1
TNBC	Triple-negative breast cancer
TGF-β	Transforming growth factor-β

Supplementary Information

The online version contains supplementary material available at https://doi.org/10.1186/s12943-024-02138-0.

Supplementary Material 1

Supplementary Material 2

Author contributions

JKR and KWL designed and performed the experiments. TK, KSH, HK, MK, DWO and GNBK assisted in experiments on cell lines. JEL performed LC-MS/MS analysis. SHP performed xenograft studies under the supervision of YJP and JY. HKK, CH, KDK and YJP provided scientific feedback, helped with data analysis, and revised the manuscript. JY provided funding, supervised the overall study, designed experiments, analyzed data, and wrote the manuscript. All authors read and approved the final manuscript.

Funding

This work was supported by the National Research Foundation of Korea (NRF) grants funded by the Korea government (MSIP) (NRF-2019R1A2C2083891 and NRF-2023R1A2C1005309 to J.Y., and NRF-2019R1I1A1A01061909 and NRF-2021R1C1C2091291 to K.J.R.).

Data availability

No datasets were generated or analysed during the current study.

Declarations

Ethics approval and consent to participate

All animal experiments were approved (Approved Number: KRIBB-AEC-21135) by the Institutional Animal Care and Use Committee of KRIBB (Ochang, Korea).

Consent for publication

Not applicable.

Competing interests

The authors declare no competing interests.

Received: 8 July 2024 / Accepted: 24 September 2024
Published online: 11 October 2024

References

1. Siegel RL, Miller KD, Jemal A. Cancer statistics, 2020. CA Cancer J Clin. 2020;70(1):7–30.
2. Bray F, Ferlay J, Soerjomataram I, Siegel RL, Torre LA, Jemal A. Global cancer statistics 2018: GLOBOCAN estimates of incidence and mortality worldwide for 36 cancers in 185 countries. CA Cancer J Clin. 2018;68(6):394–424.
3. Dent R, Trudeau M, Pritchard KI, Hanna WM, Kahn HK, Sawka CA, et al. Triple-negative breast cancer: clinical features and patterns of recurrence. Clin Cancer Res. 2007;13(15):4429–34.
4. Foulkes WD, Smith IE, Reis-Filho JS. Triple-negative breast cancer. N Engl J Med. 2010;363(20):1938–48.
5. Hudis CA, Gianni L. Triple-negative breast cancer: an unmet medical need. Oncologist. 2011;16(S1):1–11.
6. Wan L, Pantel K, Kang Y. Tumor metastasis: moving new biological insights into the clinic. Nat Med. 2013;19(11):1450–64.
7. Ikenouchi J, Matsuda M, Furuse M, Tsukita S. Regulation of tight junctions during the epithelium-mesenchyme transition: direct repression of the gene expression of claudins/occludin by Snail. J Cell Sci. 2003;116(10):1959–67.
8. Nieto MA, Huang RY, Jackson RA, Thiery JP. EMT: 2016 Cell. 2016;166(1):21–45.
9. Chaffer CL, San Juan BP, Lim E, Weinberg RA. EMT, cell plasticity and metastasis. Cancer Metastasis Rev. 2016;35(4):645–54.
10. Cano A, Perez-Moreno MA, Rodrigo I, Locascio A, Blanco MJ, del Barrio MG, et al. The transcription factor snail controls epithelial-mesenchymal transitions by repressing E-cadherin expression. Nat Cell Biol. 2000;2(2):76–83.
11. Batlle E, Sancho E, Franci C, Dominguez D, Monfar M, Baulida J, et al. The transcription factor snail is a repressor of E-cadherin gene expression in epithelial tumour cells. Nat Cell Biol. 2000;2(2):84–9.
12. Peinado H, Olmeda D, Cano A, Snail. Zeb and bHLH factors in tumour progression: an alliance against the epithelial phenotype? Nat Rev Cancer. 2007;7(6):415–28.
13. Moody SE, Perez D, Pan TC, Sarkisian CJ, Portocarrero CP, Sterner CJ, et al. The transcriptional repressor snail promotes mammary tumor recurrence. Cancer Cell. 2005;8(3):197–209.
14. Chen WJ, Wang H, Tang Y, Liu CL, Li HL, Li WT. Multidrug resistance in breast cancer cells during epithelial-mesenchymal transition is modulated by breast cancer resistant protein. Chin J Cancer. 2010;29(2):151–7.
15. Zhou BP, Deng J, Xia W, Xu J, Li YM, Gunduz M, et al. Dual regulation of snail by GSK-3beta-mediated phosphorylation in control of epithelial-mesenchymal transition. Nat Cell Biol. 2004;6(10):931–40.
16. Dominguez D, Montserrat-Sentis B, Virgos-Soler A, Guaita S, Grueso J, Porta M, et al. Phosphorylation regulates the subcellular location and activity of the snail transcriptional repressor. Mol Cell Biol. 2003;23(14):5078–89.
17. Liu Y, Zhou H, Zhu R, Ding F, Li Y, Cao X, et al. SPSB3 targets SNAIL for degradation in GSK-3β phosphorylation-dependent manner and regulates metastasis. Oncogene. 2018;37(6):768–76.
18. Zhang Y, Zhang X, Ye M, Jing P, Xiong J, Han Z, et al. FBW7 loss promotes epithelial-to-mesenchymal transition in non-small cell lung cancer through the stabilization of snail protein. Cancer Lett. 2018;419:75–83.
19. Sun R, Xie HY, Qian JX, Huang YN, Yang F, Zhang FL, et al. FBXO22 possesses both protumorigenic and antimetastatic roles in breast cancer progression. Cancer Res. 2018;78(18):5274–86.
20. Zou S, Ma C, Yang F, Xu X, Jia J, Liu Z. FBXO31 suppresses gastric cancer EMT by targeting Snail1 for proteasomal degradation. Mol Cancer Res. 2018;16(2):286–95.
21. Vinas-Castells R, Beltran M, Valls G, Gomez I, Garcia JM, Montserrat-Sentis B, et al. The hypoxia-controlled FBXL14 ubiquitin ligase targets SNAIL1 for proteasome degradation. J Biol Chem. 2010;285(6):3794–805.
22. Zheng H, Shen M, Zha YL, Li W, Wei Y, Blanco MA, et al. PKD1 phosphorylation-dependent degradation of snail by SCF-FBXO11 regulates epithelial-mesenchymal transition and metastasis. Cancer Cell. 2014;26(3):358–73.
23. Ma X, Ma X, Qiu Y, Zhu L, Lin Y, You Y, et al. TRIM50 suppressed hepatocarcinoma progression through directly targeting SNAIL for ubiquitous degradation. Cell Death Dis. 2018;9(6):608.
24. Park SM, Park SH, Ryu KJ, Kim IK, Han H, Kim HJ, et al. Downregulation of CHIP promotes ovarian cancer metastasis by inducing snail-mediated epithelial-mesenchymal transition. Mol Oncol. 2019;13(5):1280–95.

25. Wang X, De Geyter C, Jia Z, Peng Y, Zhang H. HECTD1 regulates the expression of SNAIL: implications for epithelial-mesenchymal transition. Int J Oncol. 2020;56(5):1186–98.
26. Zhang K, Corsa CA, Ponik SM, Prior JL, Piwnica-Worms D, Eliceiri KW, et al. The collagen receptor discoidin domain receptor 2 stabilizes SNAIL1 to facilitate breast cancer metastasis. Nat Cell Biol. 2013;15(6):677–87.
27. Yang Z RS, Nguyen D, Vadlamudi RK, Chen S, Kumar R. Pak1 phosphorylation of snail, a master regulator of epithelial-to-mesenchyme transition, modulates snail's subcellular localization and functions. Cancer Res. 2005;65(8):3179–84.
28. Zhang K, Rodriguez-Aznar E, Yabuta N, Owen RJ, Mingot JM, Nojima H, et al. Lats2 kinase potentiates Snail1 activity by promoting nuclear retention upon phosphorylation. EMBO J. 2012;31(1):29–43.
29. Ryu KJ, Park SM, Park SH, Kim IK, Han H, Kim HJ, et al. p38 stabilizes snail by suppressing DYRK2-mediated phosphorylation that is required for GSK3β-βTrCP-induced snail degradation. Cancer Res. 2019;79(16):4135–48.
30. Vinas-Castells R, Frias A, Robles-Lanuza E, Zhang K, Longmore GD, Garcia de Herreros A, et al. Nuclear ubiquitination by FBXL5 modulates Snail1 DNA binding and stability. Nucleic Acids Res. 2014;42(2):1079–94.
31. Choi AM, Ryter SW, Levine B. Autophagy in human health and disease. N Engl J Med. 2013;368(7):651–62.
32. Dice JF. Chaperone-mediated autophagy. Autophagy. 2007;3(4):295–9.
33. Cuervo AM, Wong E. Chaperone-mediated autophagy: roles in disease and aging. Cell Res. 2014;24(1):92–104.
34. Zhu R, Liu Y, Zhou H, Li L, Li Y, Ding F, et al. Deubiquitinating enzyme PSMD14 promotes tumor metastasis through stabilizing SNAIL in human esophageal squamous cell carcinoma. Cancer Lett. 2018;418:125–34.
35. Mingot JM, Vega S, Cano A, Portillo F, Nieto MA. eEF1A mediates the nuclear export of SNAG-containing proteins via the Exportin5-aminoacyl-tRNA complex. Cell Rep. 2013;5(3):727–37.
36. Rios J, Sequeida A, Albornoz A, Budini M. Chaperone mediated autophagy substrates and components in cancer. Front Oncol. 2021;10:614677.
37. Kumar S, Basu M, Ghosh MK. Chaperone-assisted E3 ligase CHIP: a double agent in cancer. Genes Dis. 2021;9(6):1521–55.
38. Ballinger CA, Connell P, Wu Y, Hu Z, Thompson LJ, Yin LY, et al. Identification of CHIP, a novel tetratricopeptide repeat-containing protein that interacts with heat shock proteins and negatively regulates chaperone functions. Mol Cell Biol. 1999;19(6):4535–45.
39. Connell P, Ballinger CA, Jiang J, Wu Y, Thompson LJ, Hohfeld J, et al. The co-chaperone CHIP regulates protein triage decisions mediated by heat-shock proteins. Nat Cell Biol. 2001;3(1):93–6.
40. Meacham GC, Patterson C, Zhang W, Younger JM, Cyr DM. The Hsc70 co-chaperone CHIP targets immature CFTR for proteasomal degradation. Nat Cell Biol. 2001;3(1):100–5.
41. Andrade-Tomaz M, de Souza I, Rocha CRR, Gomes LR. The role of chaperone-mediated autophagy in cell cycle control and its implications in Cancer. Cells. 2020;9(9):2140.
42. Wing SS, Chiang HL, Goldberg AL, Dice JF. Proteins containing peptide sequences related to KFERQ are selectively depleted in liver and heart, but not skeletal muscle, of fasted rats. Biochem J. 1991;275(1):165–9.
43. Cuervo AM, Knecht E, Terlecky SR, Dice JF. Activation of a selective pathway of lysosomal proteolysis in rat liver by prolonged starvation. Am J Physiol. 1995;269(5):C1200–1208.
44. Kudo N, Wolff B, Sekimoto T, Schreiner EP, Yoneda Y, Yanagida M, et al. Leptomycin B inhibition of signal-mediated nuclear export by direct binding to CRM1. Exp. Cell Res. 1998;242(2):540–7.
45. Du C, Zhang C, Hassan S, Biswas MH, Balaji KC. Protein kinase D1 suppresses epithelial-to-mesenchymal transition through phosphorylation of snail. Cancer Res. 2010;70(20):7810–9.
46. Wang H, Wang HS, Zhou BH, Li CL, Zhang F, Wang XF, et al. Epithelial-mesenchymal transition (EMT) induced by TNF-α requires AKT/GSK-3β-mediated stabilization of snail in colorectal cancer. PLoS ONE. 2013;8(2):e56664.
47. Yamasaki H, Sekimoto T, Ohkubo T, Douchi T, Nagata Y, Ozawa M, et al. Zinc finger domain of snail functions as a nuclear localization signal for importin β-mediated nuclear import pathway. Genes Cells. 2005;10(5):455–64.
48. Ko H, Kim HS, Kim NH, Lee SH, Kim KH, Hong SH, et al. Nuclear localization signals of the E-cadherin transcriptional repressor snail. Cells Tissues Organs. 2007;185(1–3):66–72.
49. Peinado H, Quintanilla M, Cano A. Transforming growth factor β-1 induces snail transcription factor in epithelial cell lines: mechanisms for epithelial mesenchymal transitions. J Biol Chem. 2003;278(23):21113–23.
50. Lv L, Li D, Zhao D, Lin R, Chu Y, Zhang H, et al. Acetylation targets the M2 isoform of Pyruvate Kinase for Degradation through chaperone-mediated autophagy and promotes Tumor Growth. Mol Cell. 2011;42(6):719–30.
51. Hormazabal J, Saavedra F, Espinoza-Arratia C, Martinez NW, Cruces T, Alfaro IE, et al. Chaperone mediated autophagy contributes to the newly synthesized histones H3 and H4 quality control. Nucleic Acids Res. 2022;50(4):1875–87.
52. Xia HG, Najafov A, Geng J, Galan-Acosta L, Han X, Guo Y, et al. Degradation of HK2 by chaperone-mediated autophagy promotes metabolic catastrophe and cell death. J Cell Biol. 2015;210(5):705–16.
53. Cuervo AM, Hu W, Lim B, Dice J. IkappaB is a substrate for a selective pathway of lysosomal proteolysis. Mol Biol Cell. 1998;9(8):1995–2010.
54. Lu TL, Huang GJ, Wang HJ, Chen JL, Hsu HP, Lu TJ. Hispolon promotes MDM2 downregulation through chaperone-mediated autophagy. Biochem Biophys Res Commun. 2010;398(1):26–31.
55. Gomes LR, Menck CFM, Cuervo AM. Chaperone-mediated autophagy prevents cellular transformation by regulating MYC proteasomal degradation. Autophagy. 2017;13(5):928–40.
56. Welsch T, Younsi A, Disanza A, Rodriguez JA, Cuervo AM, Scita G, et al. Eps8 is recruited to lysosomes and subjected to chaperone-mediated autophagy in cancer cells. Exp Cell Res. 2010;316(12):1914–24.
57. Kon M, Kiffin R, Koga H, Chapochnick J, Macian F, Varticovski L, et al. Chaperone-mediated autophagy is required for tumor growth. Sci Transl Med. 2011;3(109):109ra117.
58. Saha T. LAMP2A overexpression in breast tumors promotes cancer cell survival via chaperone-mediated autophagy. Autophagy. 2012;8(11):1643–56.
59. Zhou J, Yang J, Fan X, Hu S, Zhou F, Dong J, et al. Chaperone-mediated autophagy regulates proliferation by targeting RND3 in gastric cancer. Autophagy. 2016;12(3):515–28.
60. Quintavalle C, Di Costanzo S, Zanca C, Tasset I, Fraldi A, Incoronato M, et al. Phosphorylation-regulated degradation of the tumor-suppressor form of PED by chaperone-mediated autophagy in lung cancer cells. J Cell Physiol. 2014;229(10):1359–68.
61. Lu W, Zhang Y, McDonald DO, Jing H, Carroll B, Robertson N, et al. Dual Proteolytic Pathways Govern Glycolysis Immune Competence Cell. 2014;159(7):1578–90.
62. Xuan Y, Zhao S, Xiao X, Xiang L, Zheng HC. Inhibition of chaperone-mediated autophagy reduces tumor growth and metastasis and promotes drug sensitivity in colorectal cancer. Mol Med Rep. 2021;23(5):360.
63. Han Q, Deng Y, Chen S, Chen R, Yang M, Zhang Z, et al. Downregulation of ATG5-dependent macroautophagy by chaperone-mediated autophagy promotes breast cancer cell metastasis. Sci Rep. 2017;7(1):4759.
64. Hubbi ME, Hu H, Kshitiz, Ahmed I, Levchenko A, Semenza GL. Chaperone-mediated autophagy targets hypoxia-inducible factor-1alpha (HIF-1alpha) for lysosomal degradation. J Biol Chem. 2013;288(15):10703–14.
65. Tang J, Zhan MN, Yin QQ, Zhou CX, Wang CL, Wo LL, et al. Impaired p65 degradation by decreased chaperone-mediated autophagy activity facilitates epithelial-to-mesenchymal transition. Oncogenesis. 2017;6(10):e387.

Publisher's note